DATED HISTORY

The Mercury Rung: Dimensional Gates, Conditional Spin-2 Emergence, and Hardware Validation in QATNU

May hardware-facing design with explicit dimensional gates. The subsequent QMC and control series records the tested model and parameter window.

Manuscript · p. 1, status

Spin-2 search · null result

Evidence · Negative QATNU spin-2 search

The Mercury Rung

Dimensional Gates, Conditional Spin-2 Emergence, and Hardware Validation in QATNU

Joshua Farrow
Independent Research

May 2026

Status. This paper gives a revised Mercury-rung formulation for QATNU after the Phase-0A and Phase-1A hardware runs. The revision is stricter than the previous hardware-facing version. It places QATNU inside the known lattice-graviton and rank-2 tensor-gauge literature, adds a binding spatial-dimension gate, and demotes all currently executed two-dimensional square and triangular circuits to hardware pipeline validation rather than spin-2 admissible substrates. The current results are therefore narrower: scalar/bond signal is not gravity; raw anisotropy is not spin-2; two-dimensional embedded lattices are not hosts for a 3+1-dimensional propagating graviton; and only a pre-registered three-dimensional tensor protocol with finite-size scaling, Ward tests, dispersion exponent extraction, and source-coupling checks can pass. Phase-0A and Phase-1A remain valuable because they show that the hardware-readable QATNU encoding runs on real IBM QPUs and that the claim boundary survives noise, finite shots, transpilation, and backend replication. They do not demonstrate a derived spin-2 sector. The next admissible target is the smallest three-dimensional patch, such as a 2x2x2 cubic graph in the same v0 encoding.

Abstract

Emergent-gravity programs often succeed first at producing scalar or geometric analogies: clock slowing, graph distances, effective dimensions, raw anisotropy maps, or projection diagnostics. The hard target is different. A substrate theory of gravity must produce the dynamical spin-2 content of weak-field general relativity without inserting it by hand, while also recovering the correct dimensional and Lorentzian limits.

This paper formulates that target for the Quantum Automaton Tensor-Network Universe (QATNU), a finite local quantum substrate with matter qubits on vertices and bond registers on edges. The revised contribution is threefold. First, it situates QATNU inside existing lattice-graviton and rank-2 tensor-gauge constructions. Prior work by Gu and Wen, Xu and Hořava, Xu, Pretko, and the fracton-elasticity literature already shows that qubit, bosonic, and tensor-gauge substrates can produce graviton-like helicity-2 or rank-2 tensor sectors, often with Lifshitz or fractonic rather than relativistic dynamics. QATNU is therefore not novel merely as a lattice route to tensor modes. Its distinct contribution is a hardware-readable bond-register substrate and a staged protocol that keeps scalar/bond activation, raw tensor-looking anisotropy, Lifshitz tensor phases, and GR-like spin-2 recovery logically separate.

Second, the paper adds a spatial-dimension gate. In D spacetime dimensions a massless graviton has $D(D-3)/2$ propagating polarizations. Thus $3+1$ dimensions give two propagating helicity-2 modes, while $2+1$ dimensions give none. This reclassifies the square and triangular two-dimensional hardware runs, including the matched Kingston triangular pair, as pipeline-validation and embedded-lattice smoke tests, not spin-2 admissible substrates for the target of this paper. They show active bond/scalar observables on real hardware, but they cannot host the desired 3+1-dimensional radiative graviton even in principle.

Third, the conditional spin-2 derivation is reformulated so that the dynamical exponent is measured rather than assumed. The relativistic kernel $K_2 \sim Z_2\Omega^2 - \rho_2 k^2 - m_2^2$ is only the $z = 1$ branch. A Lifshitz branch, such as $K_2 \sim Z_z\Omega^2 - \rho_z k^{2z} - m_2^2$, is a named partial-success/failure class, motivated by prior lattice-graviton constructions. The near-term Mercury outputs are therefore the dispersion exponent z, the tensor mass/gap finite-size scaling, and a magnitude-bearing stiffness or critical exponent in microscopic bond units. The ratio $R_g = c_g/v_{\mathrm{LR}}$ is retained as a Lorentz-recovery diagnostic, with v_{LR} the Lieb-Robinson or causal-cone velocity of the substrate, not as the independent Mercury number.

The reported IBM results are kept but recontextualized. Phase-0A path, star, cycle, and diamond controls are hardware negative controls. Phase-1A house, square, and triangular circuits are hardware pipeline-validation runs. The triangular $2\times3 \to 3\times3$ Kingston pair is the strongest hardware-facing signal so far, but under the dimensional gate it remains non-admissible for a 3+1 spin-2 claim. The next result paper should run a pre-registered three-dimensional patch, beginning with a 2x2x2 cubic graph, and measure the dispersion exponent before attempting any GR-like claim.

Contents

1 The problem **3**

2 Related lattice-graviton and tensor-gauge constructions **3**

3 The Mercury criterion **4**

4 The QATNU substrate **4**

4.1 Implemented exact-diagonalization form 5

5 The scalar timing sector **6**
5.1 Weighted graph closure . . . 6
5.2 Why the scalar sector is not enough . . . 7

6 The spin-2 target **7**

7 No-go constraints **8**

8 Spatial-dimension gate **8**

9 Conditional derivation of the QATNU spin-2 sector **9**
9.1 Tensor susceptibility . . . 10
9.2 Ward residuals . . . 11
9.3 Conditional theorem . . . 11
9.4 Massless limit and source-coupling warning . . . 11

10 Phase-0A: what has now been tested **12**

11 Hardware-readable Phase-0A Hamiltonian **12**

12 Structural spin-2 admissibility gate **13**

13 Phase-0A exact-simulation controls **13**

14 Real-QPU Phase-0A hardware batch **15**
14.1 Kingston backend-consistent Phase-0A rerun . . . 17
14.2 Interpretation of the hardware batch . . . 18

15 Phase-1A: embedded graph-family hardware pipeline validation **19**
15.1 Phase-1A local Aer checks . . . 19
15.2 Phase-1 IBM hardware runs . . . 20
15.3 Kingston Phase-1A matched-family rerun . . . 21
15.4 Hardened interpretation of the triangular pair . . . 27
15.5 Interpretation of Phase 1A . . . 28

16 Reproducibility package **29**

17 What remains to make this a positive spin-2 paper **29**

18 Claim registry **30**

19 Discussion **31**

20 Conclusion **32**

A Hardware run prompt **33**

B Notation **33**

C References **33**

1 The problem

The weak-field gravitational field is not a scalar clock lag. In linearized general relativity one writes

$$g_{\mu\nu} = \eta_{\mu\nu} + h_{\mu\nu}, \qquad |h_{\mu\nu}| \ll 1, \tag{1}$$

and the propagating radiative degrees of freedom are the two transverse-traceless helicity-2 modes contained in h_{ij}^{TT}. A model that reproduces only a scalar redshift law has reproduced one observable face of weak gravity, not gravity itself.

This distinction is the central discipline of the QATNU program. The scalar sector is real enough to define, measure, and test. But the gravitational claim begins only when the substrate generates a protected spin-2 tensor sector whose equations of motion, propagator, and coupling structure match the Pauli-Fierz weak-field target.

The purpose of this paper is to put the whole story in one place. It defines the QATNU substrate, explains the scalar timing layer, derives the conditional spin-2 target, reports a first negative-control result, and gives the hardware route for reproducing the Phase-0 experiment on real quantum processors.

2 Related lattice-graviton and tensor-gauge constructions

The target of this paper is not unprecedented. The relevant prior art is not merely general emergent-gravity philosophy, but explicit lattice and tensor-gauge constructions of graviton-like sectors.

Gu and Wen constructed qubit/quantum-spin models in which linearized diffeomorphism gauge symmetry and gapless helicity ± 2 excitations can emerge at low energy. In their controlled L-type model, the helicity-± 2 modes are gapless but have a nonrelativistic dispersion proportional to k^3; a second N-type route was argued to permit linear dispersion, but without the same controlled status. Xu and Hořava obtained emergent gravity at a Gaussian $z = 3$ Lifshitz fixed point from a lattice Bose liquid, with stability tied to gauge symmetry and self-duality. Xu's algebraic Bose liquid and the later rank-2 tensor-gauge/fracton literature likewise show that symmetric tensor fields and graviton-like excitations can arise in nonfundamental media, but often with restricted mobility, Lifshitz scaling, or non-GR source behavior.

This lineage changes the QATNU claim. QATNU is not claiming to be the first lattice or qubit path to helicity-2-like excitations. The open frontier is stricter: can a hardware-readable bond-register substrate produce a three-dimensional, Lorentz-recovering, gauge-protected spin-2 sector with the source-coupling structure of weak-field gravity, rather than a Lifshitz or fracton-like tensor medium?

The lessons for the Mercury rung are:

1. A gapless tensor mode is not enough. A Lifshitz spin-2 mode with $z \neq 1$ is a scientifically interesting partial success, but not a GR-like graviton.
2. Gauge protection is preferable to critical fine tuning. A massless tensor appearing only at an isolated $\lambda_{c,2}$ is weaker than a massless sector protected by an emergent constraint or gauge redundancy over a phase.
3. Three spatial dimensions are mandatory for the target used here. Two-dimensional spatial lattices can validate hardware, scalar observables, and raw anisotropy pipelines, but they cannot host

two propagating graviton polarizations of 3+1-dimensional linearized gravity.

3 The Mercury criterion

A theory becomes more than a language when it produces an output it did not already put in. The historical role of Mercury's anomalous perihelion precession in general relativity is useful as a methodological benchmark: the decisive move was not aesthetic analogy, but a number that followed from equations constrained by other principles.

For QATNU, the corresponding requirement is:

> *derive the weak-field spin-2 sector from the substrate, including a nontrivial output number, without defining the tensor sector by the projection that one later claims to explain.*

This criterion has three parts.

1. **Known target.** The low-energy benchmark is a massless helicity-2 field with Pauli-Fierz kinetic structure and universal coupling to a conserved source.
2. **No insertion by hand.** A transverse-traceless projector may diagnose the result after the fact, but it may not be the reason the result exists.
3. **Output number.** The substrate must predict at least one number or exponent not chosen to match the answer. The near-term outputs are the dispersion exponent z, the finite-size tensor mass/gap scaling, and a magnitude-bearing tensor stiffness or critical exponent in microscopic bond units. The ratio
$$R_g = \frac{c_g}{v_{\mathrm{LR}}} \tag{2}$$
is retained as a Lorentz-recovery diagnostic once a $z = 1$ tensor branch exists, not as the independent Mercury number.

The rest of the paper is organized around this criterion.

4 The QATNU substrate

Let $G = (V, E)$ be a finite graph. Each vertex $i \in V$ carries a two-level matter system, and each edge $e = \langle i, j\rangle \in E$ carries a finite bond register. The total Hilbert space is

$$\mathcal{H} = \bigotimes_{i\in V} \mathcal{H}_i^{\mathrm{mat}} \otimes \bigotimes_{\langle i,j\rangle\in E} \mathcal{H}_{ij}^{\mathrm{bond}}, \qquad \dim \mathcal{H} = 2^{|V|}\chi_{\max}^{|E|}. \tag{3}$$

A minimal ladder Hamiltonian is

$$H = H_{\mathrm{mat}} + H_{\mathrm{bond}} + H_{\mathrm{int}}, \tag{4}$$

with

$$H_{\text{mat}} = \frac{\omega}{2} \sum_{i \in V} X_i, \tag{5}$$

$$H_{\text{bond}} = \sum_{\langle i,j \rangle} \sum_{m=0}^{\chi_{\max}-1} \epsilon_m \Pi_{ij}^{(m)}, \tag{6}$$

$$H_{\text{int}} = \lambda \sum_{\langle i,j \rangle} F_{ij} \otimes \left(R_{ij} + R_{ij}^{\dagger} \right), \tag{7}$$

$$F_{ij} = \frac{1 - Z_i Z_j}{2}, \tag{8}$$

$$R_{ij} = \sum_{m=0}^{\chi_{\max}-2} \sqrt{m+1}\, |m+1\rangle\langle m|_{ij}. \tag{9}$$

The interaction is self-referential in the limited technical sense that local matter frustration promotes or demotes the bond register that defines the medium through which matter propagates. The model is finite, local, and unitary. It is therefore a testbed for emergence, not an appeal to nonlocal collapse or external measurement.

4.1 Implemented exact-diagonalization form

The current exact-diagonalization engine implements the same architecture with matter dimension 2^N, bond dimension $\chi_{\max}^{|E|}$, lookup tables for the matter Z values, explicit edge lists, and dense Hamiltonian construction. It includes transverse matter flips, diagonal $J_0 Z_i Z_j$ matter coupling, diagonal bond energy proportional to bond rung, an optional degree penalty, and frustration-controlled bond promotion/demotion. The code-level Hamiltonian is therefore slightly more concrete than Eq. (5)–(7):

$$H_{\text{ED}} = \frac{\omega}{2} \sum_i X_i + J_0 \sum_{\langle i,j \rangle} Z_i Z_j + \Delta_B \sum_e n_e + \kappa \sum_i (d_i - k_0)^2 \tag{10}$$

$$+ \lambda \sum_{e=\langle i,j \rangle} F_{ij} \left(T_e^{+} + T_e^{-} \right), \tag{11}$$

where $T_e^{\pm}$ raise or lower the finite bond rung when allowed by the cutoff. Table 1 records the alignment between the analytic model, the exact-diagonalization implementation, and the Phase-0 hardware encoding.

Analytic object	Exact-diagonalization implementation	Hardware-readable Phase 0
Matter clocks $\frac{\omega}{2}\sum_i X_i$	Implemented as matter-state bit flips	Implemented as single-qubit X rotations
Bond ladder $\epsilon_m \Pi^{(m)}$	Linear rung energy $\Delta_B m$ with cutoff $\chi_{\max}$	One bond qubit per edge, $\chi_{\max} = 2$
Frustration tile F_{ij}	$F_{ij} = (1 - Z_i Z_j)/2$ from lookup table	Same expression compiled into controlled bond rotations
Promotion operator $R + R^\dagger$	Finite raise/lower moves of bond rung	Bond-qubit flip X_e controlled by frustration
Degree penalty	Optional $\kappa(d_i - k_0)^2$ term	Omitted in v0 to reduce depth
Tensor observable M_{ab}	Not part of legacy ED core	Raw 2D anisotropy diagnostic only

Table 1: Theory-to-code alignment. The hardware Phase-0 encoding is intentionally smaller than the full ladder theory. Its role is to test negative controls on real devices, not to complete the spin-2 derivation.

5 The scalar timing sector

The most immediate coarse observable is bond occupation. Let

$$n_{ij} = \sum_{m=0}^{\chi_{\max}-1} m \Pi_{ij}^{(m)}. \tag{12}$$

The scalar load at vertex i is

$$\Lambda_i = \sum_{j \in \partial i} \log\left(1 + \langle n_{ij} \rangle\right). \tag{13}$$

The clock law is

$$\omega_{\text{eff},i} = \frac{\omega}{1 + \alpha \Lambda_i}, \tag{14}$$

so that in weak load

$$\frac{\delta \omega_i}{\omega} \approx -\alpha \Lambda_i. \tag{15}$$

This is a valid timing sector. It is also not gravity. A scalar field can slow clocks, but it has no intrinsic transverse-traceless helicity-2 content.

5.1 Weighted graph closure

From bond occupation or dressed couplings one can extract a weighted adjacency matrix $W = (w_{ij})$ and Laplacian

$$L_w = D - W, \qquad D_{ii} = \sum_j w_{ij}. \tag{16}$$

A leading scalar closure is

$$(\kappa L_w + \mu^2 I)\Lambda = A\rho, \tag{17}$$

with dynamical completion

$$\partial_t \Lambda + \Gamma(\kappa L_w + \mu^2 I)\Lambda = \Gamma A \rho(t). \tag{18}$$

If $L_w\phi_n = \lambda_n\phi_n$, the relaxation rates should satisfy

$$\tau_n^{-1} = \Gamma(\kappa\lambda_n + \mu^2). \tag{19}$$

The same operator defines a diffusion return probability,

$$P_{\mathrm{return}}(t) = \frac{1}{|V|}\mathrm{Tr}\, e^{-tL_w}, \tag{20}$$

and an effective dimension,

$$d_{\mathrm{eff}}^{(\mathrm{diff})}(t) = -2\frac{d\log P_{\mathrm{return}}(t)}{d\log t}. \tag{21}$$

A shell profile gives an independent estimator,

$$d_{\mathrm{eff}}^{(\Lambda)}(r) = 2 - \frac{d\log|\Lambda_{\mathrm{shell}}(r)|}{d\log r}. \tag{22}$$

The severe scalar closure test is therefore

$$d_{\mathrm{eff}}^{(\mathrm{diff})} \approx d_{\mathrm{eff}}^{(\Lambda)} \approx 3 \tag{23}$$

in the same window where Eq. (14) fits best.

5.2 Why the scalar sector is not enough

For a scalar load Λ_i, the discrete difference on an oriented edge is

$$(d\Lambda)_{ij} = \Lambda_j - \Lambda_i. \tag{24}$$

Around any closed loop $\gamma = (i_0, i_1, \ldots, i_m = i_0)$,

$$\sum_{a=0}^{m-1}(d\Lambda)_{i_a i_{a+1}} = \sum_{a=0}^{m-1}(\Lambda_{i_{a+1}} - \Lambda_{i_a}) = 0. \tag{25}$$

The scalar timing sector is holonomy-free in this sense. It cannot by itself represent gravitomagnetic circulation, transverse-traceless gravitational waves, or the constraint structure of linearized general relativity.

This is not a defect of the scalar sector. It is its boundary.

6 The spin-2 target

The weak-field benchmark is the Pauli-Fierz theory of a massless spin-2 field. For a symmetric perturbation $h_{\mu\nu}$ with trace $h = \eta^{\mu\nu}h_{\mu\nu}$, the quadratic Lagrangian density can be written as

$$\mathcal{L}_{\mathrm{PF}} = \frac{1}{2}\partial_\lambda h_{\mu\nu}\partial^\lambda h^{\mu\nu} - \partial_\mu h^{\mu\nu}\partial^\lambda h_{\lambda\nu} + \partial_\mu h^{\mu\nu}\partial_\nu h - \frac{1}{2}\partial_\lambda h\partial^\lambda h. \tag{26}$$

It is invariant under the linearized gauge transformation

$$h_{\mu\nu} \mapsto h_{\mu\nu} + \partial_\mu\xi_\nu + \partial_\nu\xi_\mu. \tag{27}$$

In the source-free transverse-traceless sector,

$$\partial_i h_{ij}^{\mathrm{TT}} = 0, \qquad \delta^{ij} h_{ij}^{\mathrm{TT}} = 0, \tag{28}$$

and the wave equation is

$$\left(\partial_t^2 - c_g^2 \nabla^2\right) h_{ij}^{\mathrm{TT}} = 0. \tag{29}$$

The TT projector in momentum space is

$$\Pi_{ij}(\mathbf{k}) = \delta_{ij} - \frac{k_i k_j}{k^2}, \tag{30}$$

$$P_{ij,kl}^{\mathrm{TT}}(\mathbf{k}) = \frac{1}{2}\left(\Pi_{ik}\Pi_{jl} + \Pi_{il}\Pi_{jk} - \Pi_{ij}\Pi_{kl}\right). \tag{31}$$

This projector is allowed as a diagnostic. It is not allowed as the generator of the claimed physics.

7 No-go constraints

The spin-2 target is constrained by the Weinberg-Witten obstruction. An ordinary Lorentz-invariant quantum field theory with a Lorentz-covariant conserved stress tensor cannot contain a composite massless spin greater than one particle that carries that stress tensor in the usual way. The point is not that emergent gravity is impossible. The point is that any successful route must explain why the theorem's assumptions fail microscopically while the correct Lorentz and gauge structure reappears in the infrared.

QATNU has a possible route because its microscopic theory is not a continuum Lorentz-covariant field theory. It begins from a finite graph, local update rules, and bond registers. But this is not enough. A preferred microscopic graph only avoids one assumption. The model must still demonstrate:

1. an emergent limiting tensor-wave speed with decreasing anisotropy at long wavelength;
2. an emergent gauge or constraint structure that removes nonphysical polarizations;
3. an effective conserved source that appears in the same infrared limit.

Without these, a tensor mode in QATNU would be a medium excitation, not gravitational spin-2.

8 Spatial-dimension gate

The spin-2 target in this paper is the weak-field graviton of $3+1$-dimensional general relativity. This imposes a hard dimensional requirement. In D spacetime dimensions, a massless spin-2 field has

$$N_{\mathrm{pol}}(D) = \frac{D(D-3)}{2} \tag{32}$$

propagating polarizations. For $D = 4$, $N_{\mathrm{pol}} = 2$. For $D = 3$, corresponding to a two-dimensional spatial lattice plus time, $N_{\mathrm{pol}} = 0$.

This is not a minor finite-size caveat. A square or triangular sheet may have meaningful scalar loads, bond anisotropy, and two-dimensional tensor algebra, but it is not an admissible host for the two propagating helicity-2 modes targeted by Eq. (31). In $2+1$ gravity the Einstein theory is

topological in the sense relevant here: there are no local gravitational waves. Therefore all currently executed two-dimensional square and triangular circuits must be classified as pipeline-validation runs, not as spin-2 admissible candidates for the $3+1$ Mercury target.

The graph-family gate is now:

1. **Phase-0A controls:** path, star, cycle, rhombus/diamond, and other small motifs. These validate rejection and hardware readout.
2. **Phase-1A two-dimensional validation:** house, square, and triangular patches. These validate embedded graph hardware, scalar/bond readout, and raw anisotropy maps, but fail the $3+1$ spin-2 admissibility gate.
3. **Phase-1B first admissible candidates:** three-dimensional patches with a low-k window, beginning with a 2x2x2 cubic graph and then extending to 2x2x3, 3x3x2, and larger families.

In the current v0 hardware encoding, with one matter qubit per vertex and one bond qubit per edge, the first few cubic patches are modest relative to 156-qubit IBM Heron-class backends:

3D patch	vertices	edges	hardware qubits	role
2x2x2 cubic	8	12	20	first 3D admissibility smoke test
2x2x3 cubic	12	20	32	first elongated scaling check
3x3x2 cubic	18	33	51	first broad low-k patch

Table 2: First three-dimensional QATNU targets in the v0 hardware encoding. These are the first graph families that can even attempt the 3+1-dimensional spin-2 target.

The earlier scalar closure standard also points in the same direction. The scalar sector requires agreement between diffusion-based and shell-profile effective dimensions in the same window. A two-dimensional shell response or a two-dimensional hardware sheet cannot be silently upgraded into a three-dimensional tensor continuum.

9 Conditional derivation of the QATNU spin-2 sector

The natural tensor candidate is not built from the scalar load itself. It is built from anisotropic bond stress. On an admissible graph family, a tensor observable first requires a chart. For hardware fixtures this may be an explicit embedding; for an emergent-geometry claim it must also be reproduced by an intrinsic chart, such as a spectral or diffusion-map embedding derived from L_w. Let each edge e have unit tangent $\hat{t}_e$ and centered occupation

$$q_e = n_e - \langle n \rangle_{\mathcal{N}(x)}. \tag{33}$$

In a coarse cell $\mathcal{N}(x)$ define the symmetric traceless tensor

$$M_{ab}(x) = \sum_{e \in \mathcal{N}(x)} q_e \left(\hat{t}_{e,a} \hat{t}_{e,b} - \frac{1}{d} \delta_{ab} \right). \tag{34}$$

This is a substrate observable. It is not made transverse-traceless by definition. However, it is not yet an intrinsic geometric observable unless the result is stable under allowed chart choices. Chart stability is therefore a gate, not a decorative robustness check.

9.1 Tensor susceptibility

Couple a weak source J_{ab} to M_{ab}:

$$H_J = -\sum_x J_{ab}(x) M_{ab}(x). \tag{35}$$

Equivalently, at the edge level, the bond energy is biased as

$$\Delta_B(e) \mapsto \Delta_B - J_{ab}(x_e)\left(\hat{t}_{e,a}\hat{t}_{e,b} - \frac{1}{d}\delta_{ab}\right). \tag{36}$$

Define the connected susceptibility

$$\chi_{ab,cd}(\Omega, \mathbf{k}) = \frac{\delta\langle M_{ab}(\Omega, \mathbf{k})\rangle}{\delta J_{cd}(\Omega, \mathbf{k})}. \tag{37}$$

The inverse tensor kernel is

$$K_{ab,cd}(\Omega, \mathbf{k}) = \chi^{-1}_{ab,cd}(\Omega, \mathbf{k}). \tag{38}$$

In the tensor channel one must not assume the relativistic branch. The two leading possibilities to distinguish are

$$K_2^{(z=1)}(\Omega, k) = Z_2\Omega^2 - \rho_2 k^2 - m_2^2 + O(k^4, \Omega^4, k^2\Omega^2), \tag{39}$$

$$K_2^{(z)}(\Omega, k) = Z_z\Omega^2 - \rho_z k^{2z} - m_2^2 + \cdots, \tag{40}$$

where z is the dynamical exponent. The $z = 1$ form is the GR-like target; $z = 2$ or $z = 3$ would place QATNU in a Lifshitz/tensor-medium class rather than the relativistic Pauli-Fierz class. A perturbative fast-sector elimination gives the schematic tensor mass

$$m_2^2(\lambda) = \Delta_B^{(2)} - \lambda^2\Pi_2(0, 0) + O(\lambda^4), \tag{41}$$

where $\Pi_2(0, 0)$ is the zero-frequency tensor polarization of the matter/frustration sector. Hence the tensor critical point is

$$m_2^2 = 0 \qquad \Longleftrightarrow \qquad \lambda_{c,2}^2 = \frac{\Delta_B^{(2)}}{\Pi_2(0, 0)} + O(\lambda_{c,2}^4). \tag{42}$$

At criticality, the pole condition gives

$$\Omega^2 \sim \frac{\rho_z}{Z_z} k^{2z}. \tag{43}$$

Only on the relativistic branch $z = 1$ can one define

$$\Omega^2 = c_g^2 k^2 + O(k^4), \qquad c_g^2 = \frac{\rho_2}{Z_2}. \tag{44}$$

The Lorentz-recovery diagnostic is then

$$R_g = \frac{c_g}{v_{\mathrm{LR}}} = \frac{1}{v_{\mathrm{LR}}}\sqrt{\frac{\rho_2}{Z_2}}, \tag{45}$$

where v_{LR} is the Lieb-Robinson or causal-cone velocity of the same substrate in the same microscopic units. The dispersion exponent z and the finite-size scaling of m_2 are the first Mercury outputs; R_g is meaningful only after a $z = 1$ branch has been established.

9.2 Ward residuals

A massless tensor in a medium is not automatically a graviton. The nonphysical modes must decouple. Define the residuals

$$\mathcal{W}_{\mathrm{div}}(k) = \frac{\|k^a \chi_{ab,cd}\|}{\|\chi_{ab,cd}\|}, \qquad \mathcal{W}_{\mathrm{tr}}(k) = \frac{\|\delta^{ab}\chi_{ab,cd}\|}{\|\chi_{ab,cd}\|}. \tag{46}$$

The infrared Ward condition is

$$\mathcal{W}_{\mathrm{div}}(k) \to 0, \qquad \mathcal{W}_{\mathrm{tr}}(k) \to 0 \qquad (k \to 0). \tag{47}$$

If Eq. (41) reaches a protected massless regime, Eq. (46) vanishes, and the measured exponent is $z = 1$, the long-wavelength correlator takes the form

$$\langle M_{ab}(\Omega, \mathbf{k}) M_{cd}(-\Omega, -\mathbf{k})\rangle_c \sim \frac{Z\, P^{\mathrm{TT}}_{ab,cd}(\mathbf{k})}{\Omega^2 - c_g^2 k^2 + i0} + \text{analytic terms}. \tag{48}$$

The TT projector appears here as the consequence of the infrared constraints, not as the definition of M_{ab}.

9.3 Conditional theorem

Conditional spin-2 theorem. *Suppose a QATNU graph family is three-dimensional in the infrared, admits both explicit and intrinsic charts for M_{ab}, has a tensor inverse kernel whose measured dynamical exponent is $z = 1$, reaches a protected massless tensor regime, and satisfies vanishing Ward residuals Eq. (46). Then the radiative long-wavelength sector has two transverse-traceless propagating degrees of freedom, wave speed $c_g^2 = \rho_2/Z_2$, and a local quadratic effective action equivalent to Pauli-Fierz up to field normalization.*

This theorem is conditional, but it is not empty. It names the quantities that must be computed: $\Pi_2(0,0)$, Z_z, ρ_z, z, the finite-size scaling of m_2, chart-stability residuals, Ward residuals, and only then R_g. It also names the likely partial success: a gapless gauge-protected tensor mode with $z \neq 1$ is a Lifshitz spin-2 medium, not a GR-like graviton.

9.4 Massless limit and source-coupling warning

A vanishing fitted tensor mass is not enough. Massive spin-2 responses can fail to approach the massless source-coupling structure smoothly; the extra scalar polarization can survive in the massless limit. The propagator pole test and the universal-source-coupling test are therefore logically independent. A QATNU tensor branch must test both.

10 Phase-0A: what has now been tested

The full tensor theorem requires large embedded graph families and finite-size scaling. The present hardware-accessible test is smaller and more conservative. Phase 0A asks whether the QATNU circuit and analysis pipeline can do three things at once:

1. run a hardware-readable QATNU circuit;
2. extract nonzero bond and scalar observables;
3. refuse a spin-2 interpretation for a topology that is structurally inadmissible.

The third point is the key. This is a structural admissibility gate, not a dynamical tensor susceptibility measurement. It asks whether the graph/circuit is even eligible to host an infrared transverse-traceless sector. A one-dimensional path fails before any hardware counts are examined. The hardware counts then test a different claim: whether the QATNU encoding and scalar/bond readout are live on a real backend.

11 Hardware-readable Phase-0A Hamiltonian

For real quantum hardware, the bond ladder is reduced to one bond qubit per edge, so $\chi_{\max} = 2$. The Hilbert space is

$$\mathcal{H}_{\mathrm{v0}} = (\mathbb{C}^2)^{\otimes(|V|+|E|)}. \tag{49}$$

The Hamiltonian is

$$H_{\mathrm{v0}} = H_{\mathrm{mat}} + H_{ZZ} + H_{\mathrm{bond}} + H_{\mathrm{prom}}, \tag{50}$$

with

$$H_{\mathrm{mat}} = \frac{\omega}{2} \sum_{i \in V} X_i, \tag{51}$$

$$H_{ZZ} = J_0 \sum_{\langle i,j \rangle \in E} Z_i Z_j, \tag{52}$$

$$H_{\mathrm{bond}} = \Delta_B \sum_{e \in E} n_e, \qquad n_e = \frac{I - Z_e}{2}, \tag{53}$$

$$H_{\mathrm{prom}} = \lambda \sum_{e=\langle i,j \rangle} F_{ij} X_e, \qquad F_{ij} = \frac{1 - Z_i Z_j}{2}. \tag{54}$$

The initial state is

$$|\psi_0\rangle = |+\rangle^{\otimes|V|} \otimes |0\rangle^{\otimes|E|}. \tag{55}$$

The parameters used here are

$$\omega = 1.0, \qquad J_0 = 0.12, \qquad \Delta_B = 0.55, \qquad \lambda = 0.35, \qquad T = 2.0. \tag{56}$$

Bond occupation, scalar load, load spread, raw anisotropy, and the many-body ground gap are computed after exact statevector evolution. For embedded two-dimensional controls the raw

anisotropy diagnostic is

$$M_{ab}^{(2D)} = \sum_e q_e \left(\hat{t}_{e,a} \hat{t}_{e,b} - \frac{1}{2} \delta_{ab} \right), \qquad q_e = \langle n_e \rangle - \frac{1}{|E|} \sum_f \langle n_f \rangle. \tag{57}$$

This diagnostic is not a TT derivation. It only checks whether a small control graph exercises a nonzero centered directional tensor channel.

12 Structural spin-2 admissibility gate

The corrected Phase-0A predicate has four stages.

1. It computes the centered bond pattern q_e and raw anisotropy M_{ab}.
2. It records whether the tensor channel is actually exercised, i.e. whether q_e and M_{ab} are nonzero above numerical tolerance.
3. It checks whether the graph family has a three-dimensional spatial infrared limit, not merely a two-dimensional embedding.
4. It checks whether the graph is large enough to have a meaningful low-k infrared window.

This predicate can return different kinds of no. A path can fail because the tensor channel is not exercised and because the chart has rank one. A chorded diamond, bowtie, square sheet, or triangular sheet can exercise a nonzero two-dimensional anisotropy tensor and still fail because a two-dimensional spatial graph has no 3+1-dimensional helicity-2 infrared limit. This is better than a hardcoded failure label: it records why the graph is rejected.

13 Phase-0A exact-simulation controls

Table 3 gives the corrected exact statevector controls. The diamond control is the chorded plaquette, K_4 minus one edge, and is no longer identical to the cycle. The bowtie/kite control is included as a second nonzero two-dimensional tensor-channel negative control.

Graph	Edges	Qubits	$\langle n_e \rangle$	$\Delta\Lambda$	$\sum \lvert q_e \rvert$	Chart rank	Phase-0A result
Path	3	7	0.12878	0.12278	0.00371	1	null tensor channel
Cycle	4	8	0.13015	0.00000	0.00000	2	null tensor channel
Star	3	7	0.13050	0.24532	0.00000	2	null tensor channel
Diamond	5	9	0.12800	0.11933	0.00251	2	non-3D tensor control
Bowtie	5	9	0.12800	0.11933	0.00251	2	non-3D tensor control

Table 3: Corrected Phase-0A exact controls. Path, cycle, and star do not exercise a usable tensor channel. Chorded diamond and bowtie exercise a nonzero two-dimensional tensor channel but still fail the spin-2 admissibility gate because they are not three-dimensional infrared substrates.

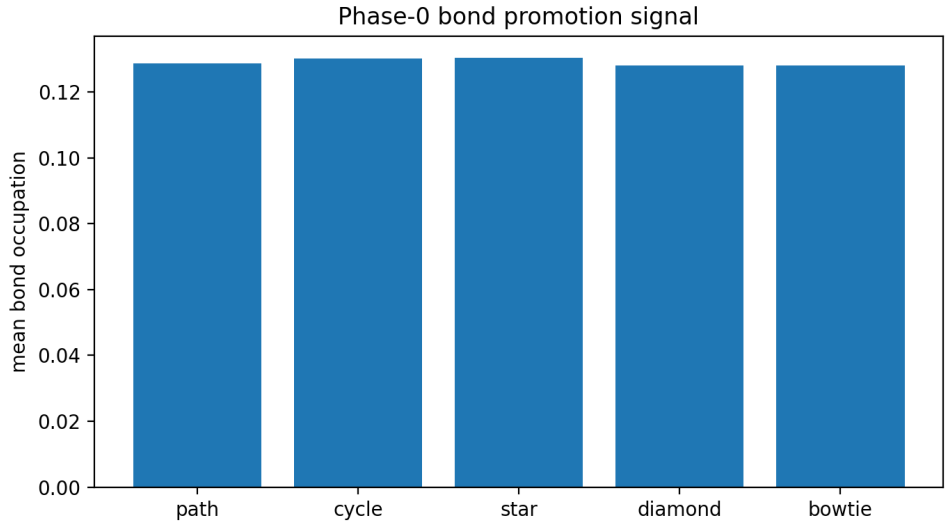

Figure 1: Mean bond occupation after exact evolution. The bond/scalar sector is active in all controls.

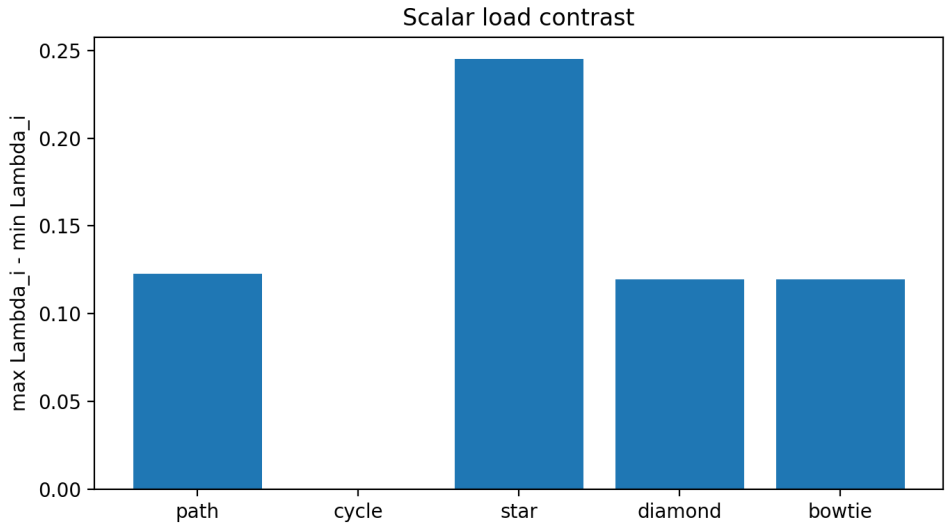

Figure 2: Scalar load spread for the corrected exact controls. The path, star, chorded diamond, and bowtie generate nonuniform scalar load; the symmetric cycle is uniform under the chosen state and parameters.

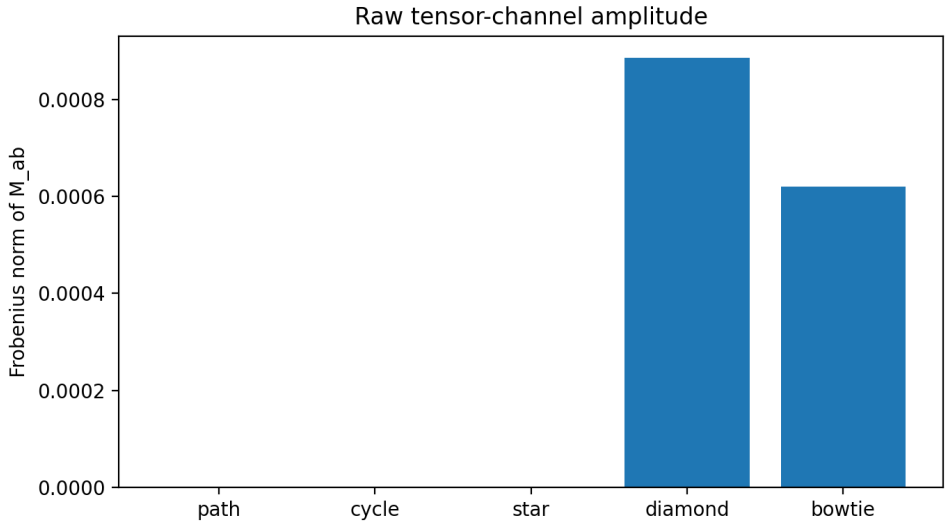

Figure 3: Raw anisotropy Frobenius norm. The nonzero values for chorded diamond and bowtie show that the tensor-channel diagnostic is being exercised, but these controls remain structurally inadmissible for spin-2 gravity.

14 Real-QPU Phase-0A hardware batch

The completed Phase-0A hardware batch ran four negative-control circuits on IBM Quantum hardware. The circuits are hardware-readable QATNU encodings with one matter qubit per vertex and one bond qubit per edge. The purpose of the batch is not to discover gravity. It is to test whether active scalar/bond signals survive real backend execution while the spin-2 admissibility gate continues to refuse inadmissible topologies.

Topology	Backend	Job ID	Circuit role	$\langle n_e \rangle_{\mathrm{IBM}}$	Verdict
Path	`ibm_marrakesh`	`d8b6och59p8c73bm3fog`	1D null tensor channel	0.196833	fail expected
Star	`ibm_fez`	`d8b6tfke6kns73aalim0`	hub/no smooth IR limit	0.181000	fail expected
Cycle	`ibm_marrakesh`	`d8b6vm4e6kns73aallj0`	finite ring/no 3D IR	0.191875	fail expected
Diamond	`ibm_marrakesh`	`d8b6vrce6kns73aalls0`	finite plaquette control	0.156875	fail expected

Table 4: Completed IBM Phase-0A hardware batch. All four controls produced nonzero mean bond occupation and all four retained the expected negative-control verdict. The batch validates hardware execution and claim discipline, not a positive spin-2 sector.

The batch result can be summarized as

```
IBM Phase-0A batch:
active scalar/bond signal: yes, all four controls
spin-2 admissible substrate: no, all four controls
verdict: FAIL_EXPECTED_NEGATIVE_CONTROL, all four controls
```

For the path run, raw counts were also analyzed in detail. The path circuit used seven qubits, ran

on `ibm_marrakesh`, completed with 2000 shots and 118 distinct measured bitstrings, and produced

$$\langle n_e \rangle_{\mathrm{IBM}} = [0.1905,\ 0.1585,\ 0.2415], \tag{58}$$

$$\Lambda_{\mathrm{IBM}} = [0.17437,\ 0.32150,\ 0.36345,\ 0.21632]. \tag{59}$$

The mean bond occupation was 0.19683 and the scalar-load spread was 0.18907. Thus the hardware circuit was not dead: it produced active bond occupation and nonuniform scalar load. The structural spin-2 gate still rejected it because a path has no transverse-traceless helicity-2 sector.

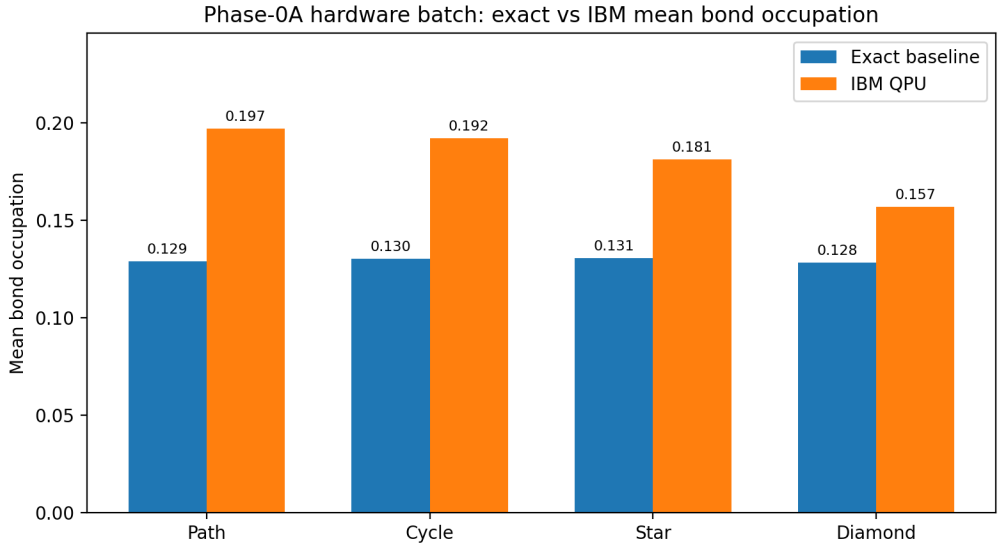

Figure 4: Exact baseline versus IBM mean bond occupation for the completed Phase-0A hardware batch. The IBM runs show active bond occupation across all four controls, while every topology remains structurally inadmissible for spin-2.

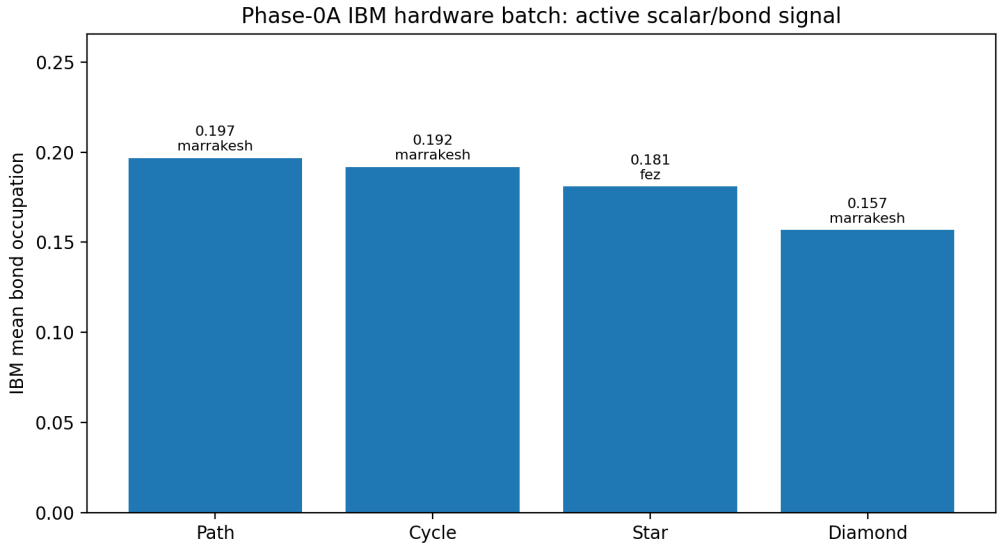

Figure 5: IBM-only mean bond occupation for the Phase-0A batch. Backend variation and hardware noise are treated as execution effects, not as new physics. The scientific result is the survival of the claim boundary.

14.1 Kingston backend-consistent Phase-0A rerun

After the first mixed-backend Phase-0A batch, the same four controls were rerun on `ibm_kingston`. This rerun is a backend-consistency check, not a new physics regime. It asks whether the Mercury-rung refusal layer survives when all four controls are executed on the same backend, with the same shot count and result extractor.

Topology	Backend	Job ID	Shots	$\langle n_e \rangle$	$\Delta\Lambda$	Verdict
Path	`ibm_kingston`	`d8b79k5mdd1s73b95ncg`	2000	0.170500	0.171082	fail expected
Star	`ibm_kingston`	`d8b79qh59p8c73bm46jg`	2000	0.203500	0.398831	fail expected
Cycle	`ibm_kingston`	`d8b7a1159p8c73bm46qg`	2000	0.181500	0.076928	fail expected
Diamond	`ibm_kingston`	`d8b7a6ce6kns73aam35g`	2000	0.158500	0.025118	fail expected

Table 5: Backend-consistent Kingston rerun of the Phase-0A controls. The numeric observables shift relative to the first mixed-backend batch, but the verdict structure is unchanged: every control has active bond/scalar readout and every control remains structurally inadmissible for a spin-2 claim.

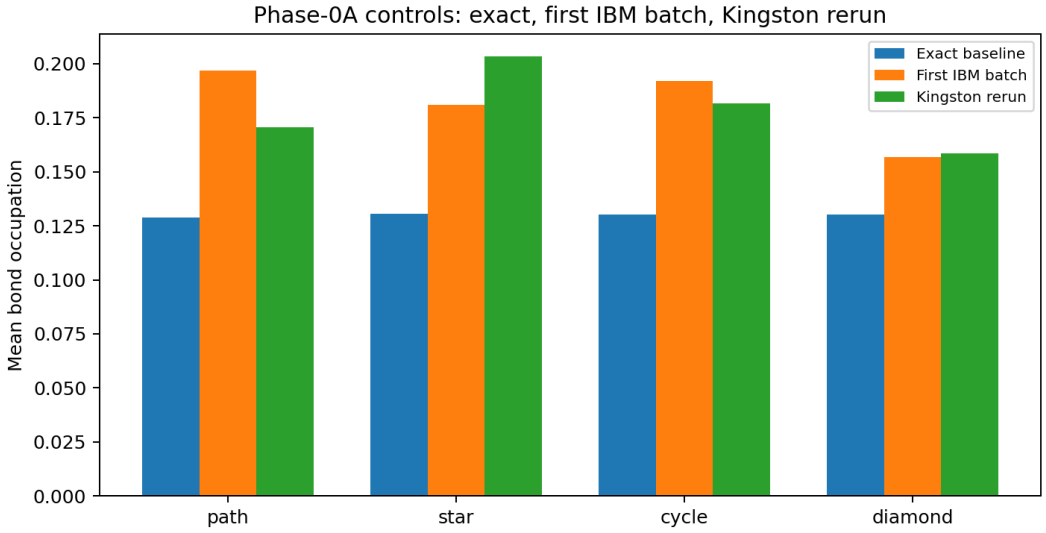

Figure 6: Phase-0A mean bond occupation across exact baselines, the first IBM batch, and the Kingston rerun. Backend-to-backend variation is visible, but the claim boundary is invariant.

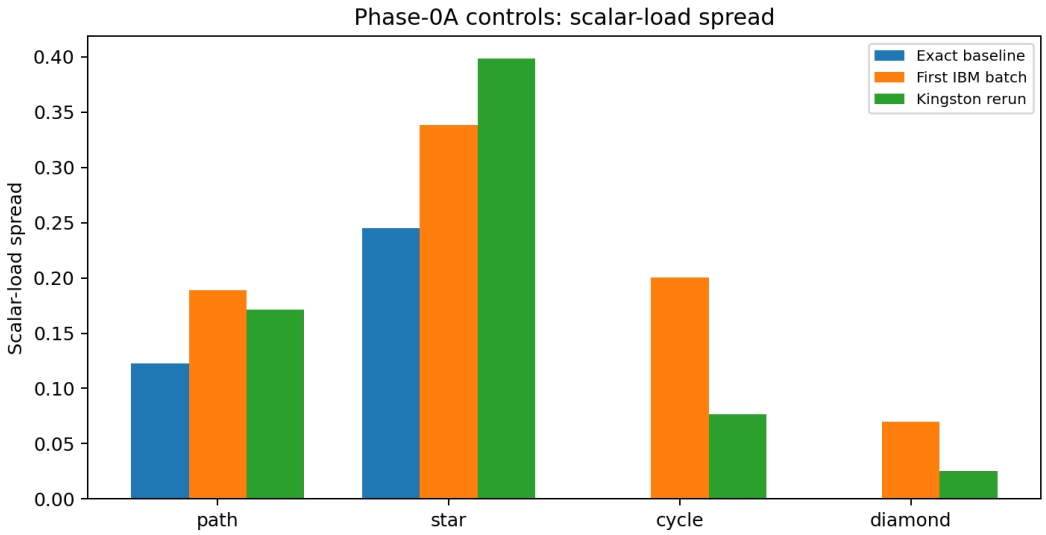

Figure 7: Phase-0A scalar-load spread across exact baselines, the first IBM batch, and the Kingston rerun. The hardware spread is device-sensitive; it is not interpreted as a tensor signal.

The Kingston rerun preserves the essential Phase-0A result:

```
active scalar/bond signal: yes, all controls
spin-2 admissible substrate: no, all controls
verdict: FAIL_EXPECTED_NEGATIVE_CONTROL, all controls
```

14.2 Interpretation of the hardware batch

The correct result statement is:

Four QATNU Phase-0A negative-control circuits ran on real IBM Quantum hardware. Each produced nonzero bond/scalar signal. Each was rejected by the structural spin-2 admissibility gate. The batch therefore validates the hardware-readable encoding, the bond/scalar readout, and the claim boundary, but it does not measure a dynamical tensor susceptibility or provide positive spin-2 evidence.

This strengthens the Mercury-rung discipline. Before asking whether QATNU can derive a spin-2 sector, the protocol must show that it does not automatically hallucinate spin-2 from promoted-bond activity. The completed hardware batch provides that "no" on real devices.

15 Phase-1A: embedded graph-family hardware pipeline validation

The Phase-1A graph-family pass extends the isolated hardware-prep package beyond the original Phase-0A negative controls. It still uses the hardware-readable v0 encoding: one matter qubit per vertex, one bond qubit per edge, four Trotter steps, and total evolution time $T = 2.0$. It does not yet couple these circuits back into the full exact-diagonalization pipeline, and it does not yet extract a tensor susceptibility. Under the spatial-dimension gate, these two-dimensional graph families are now classified as hardware pipeline-validation runs rather than spin-2 admissible candidates.

The purpose of Phase 1A is narrower: test whether larger, embedded graph families can be compiled, locally simulated, and run on real IBM hardware while preserving the Mercury-rung claim boundary. The role labels are therefore deliberately conservative.

Topology	Vertices	Edges	Qubits	Role
`house`	5	6	11	small non-1D motif negative control
`square_2x3`	6	7	13	2D square-lattice validation
`triangular_2x3`	6	9	15	2D triangular-lattice validation
`square_3x3`	9	12	21	2D square-lattice scaling smoke test; hardware smoke test after smaller circuits
`triangular_3x3`	9	16	25	2D triangular-lattice smoke test; not 3D-admissible

Table 6: Phase-1A graph families. The square and triangular entries are embedded 2D validation families, not 3D spin-2 admissible substrates. The 21-qubit `square_3x3` and 25-qubit `triangular_3x3` circuits extend the smoke tests into matched same-backend graph-family pairs.

15.1 Phase-1A local Aer checks

Local Aer checks show active bond/scalar observables for each family. The verdict labels are claim-boundary labels: house remains a negative control, while the embedded square and triangular families are candidate substrates requiring finite-size scaling and tensor-channel analysis.

Topology	Shots	$\langle n_e \rangle$	$\Delta\Lambda$	Raw anis.	Verdict
`house`	2000	0.133000	0.145126	0.278450	fail expected
`square_2x3`	2000	0.135000	0.146430	0.489535	candidate, not claimed
`triangular_2x3`	2000	0.139611	0.275658	0.449204	candidate, not claimed
`square_3x3`	512	0.134115	0.241870	0.294628	candidate, not claimed

Table 7: Phase-1A local Aer checks. Nonzero bond occupation, scalar-load spread, and raw anisotropy appear across the family, but these are still scalar/bond and raw geometry diagnostics, not a spin-2 susceptibility.

15.2 Phase-1 IBM hardware runs

The first Phase-1A hardware pass submitted the graph-family circuits to IBM Quantum with 2000 shots each. The initial smaller circuits established that non-1D and embedded 2D candidates could run; the 21-qubit `square_3x3` circuit was then submitted as a larger square-family hardware smoke test. All submitted jobs used Qiskit Runtime on the IBM Quantum Platform channel.

Topology	Backend	Job ID	$\langle n_e \rangle$	$\Delta\Lambda$	Raw anis.	Verdict
`house`	`ibm_marrakesh`	`d8b75h6honmc73cjjql0`	0.188917	0.193522	0.518695	fail expected
`square_2x3`	`ibm_marrakesh`	`d8b75b159p8c73bm4180`	0.165929	0.262930	0.311503	candidate, not claimed
`triangular_2x3`	`ibm_marrakesh`	`d8b75m159p8c73bm41l0`	0.177611	0.627958	0.431851	candidate, not claimed
`square_3x3`	`ibm_marrakesh`	`d8b77kehonmc73cjjt8g`	0.171500	0.530356	0.457432	candidate, not claimed

Table 8: Phase-1A IBM hardware pass. The embedded 2D graph families run and return active observables, but the results are not spin-2 evidence. They establish hardware reach for candidate graph families and identify the next analysis burden.

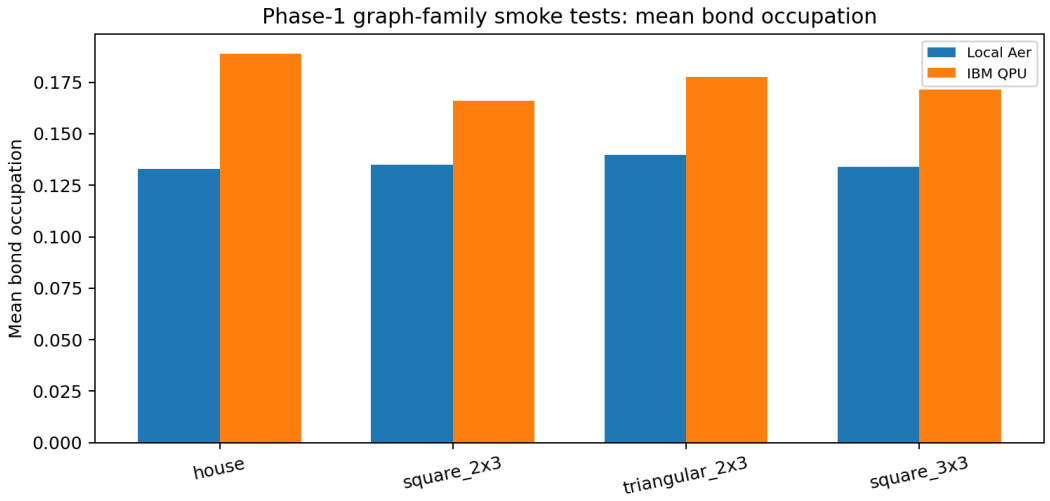

Figure 8: Phase-1A mean bond occupation. IBM values are higher than local Aer for the submitted circuits, consistent with hardware/transpilation/noise sensitivity rather than new physics.

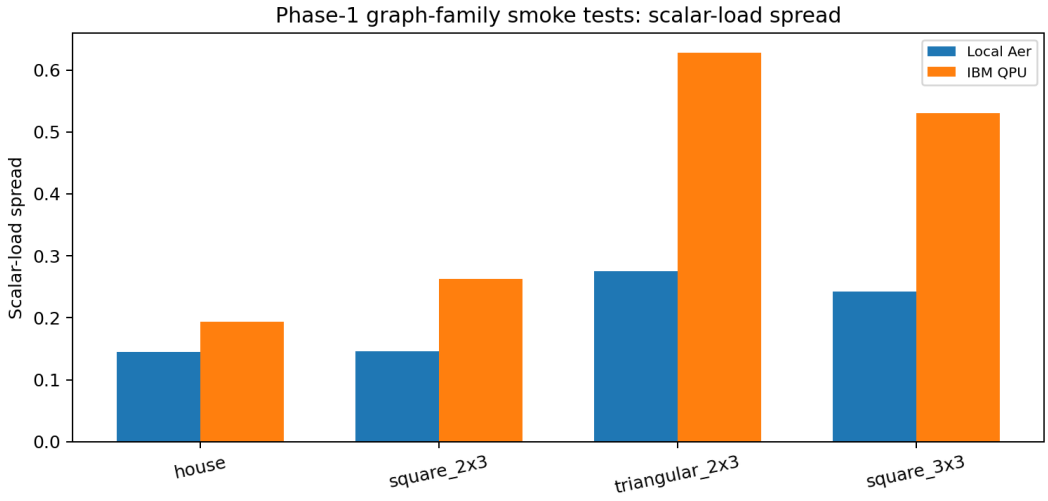

Figure 9: Phase-1A scalar-load spread. The triangular_2x3 hardware run shows a much larger scalar-load spread than local Aer. This should be treated as device- and layout-sensitive until repeated with calibration metadata and mitigation.

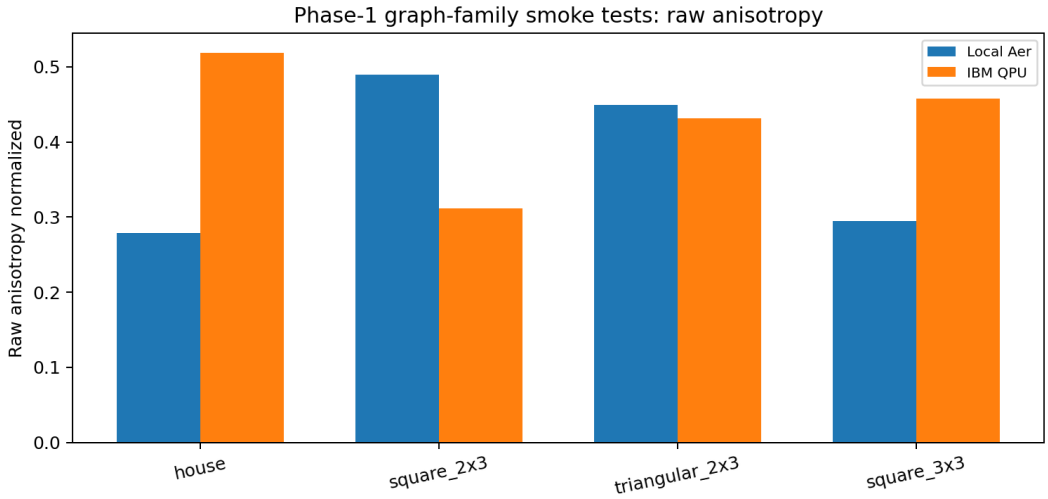

Figure 10: Phase-1A raw anisotropy diagnostic. Raw anisotropy is useful for checking that the graph-family readout is not trivial, but it is not a tensor susceptibility and cannot support a spin-2 claim on its own.

15.3 Kingston Phase-1A matched-family rerun

After the first Marrakesh pass, the Phase-1 house control, square family, and triangular family were checked on `ibm_kingston`. The house job reached `DONE` and was retrieved; no duplicate house job was submitted. This gives the cleanest Phase-1 comparison so far because `house`, `square_2x3`, `square_3x3`, `triangular_2x3`, and `triangular_3x3` share backend, shot count, Trotter settings, and result extractor. It is still not a finite-size spin-2 result: there is only one shot batch per size, no fixed physical layout policy, no mitigation, no backend-calibration metadata inside the result

object, and no tensor-channel observable. But it is a real hardware reach result: the same QPU path now executes the 21-qubit square and 25-qubit triangular candidates.

Topology	Backend	Job ID	Shots	$\langle n_e \rangle$	$\Delta\Lambda$	Raw anis.	Verdict
`house`	`ibm_kingston`	`d8b7bh5mdd1s73b95pg0`	2000	0.148167	0.176631	0.378877	fail expected
`square_2x3`	`ibm_kingston`	`d8b7acce6kns73aam3d0`	2000	0.179357	0.432255	0.485347	candidate, not claimed
`square_3x3`	`ibm_kingston`	`d8b7ahse6kns73aam3jg`	2000	0.178042	0.347370	0.066164	candidate, not claimed
`triangular_2x3`	`ibm_kingston`	`d8b7o4h59p8c73bm4ung`	2000	0.205333	0.645560	0.417111	candidate, not claimed
`triangular_3x3`	`ibm_kingston`	`d8b7ps4e6kns73aamsmg`	2000	0.256438	1.520218	0.133410	candidate, not claimed

Table 9: Kingston Phase-1A matched-family rerun. The house control remains a negative control on the same backend, while the square and triangular pairs execute and remain analyzable. None of these rows is promoted to spin-2 evidence; the result is hardware reach plus claim discipline, not a tensor pole.

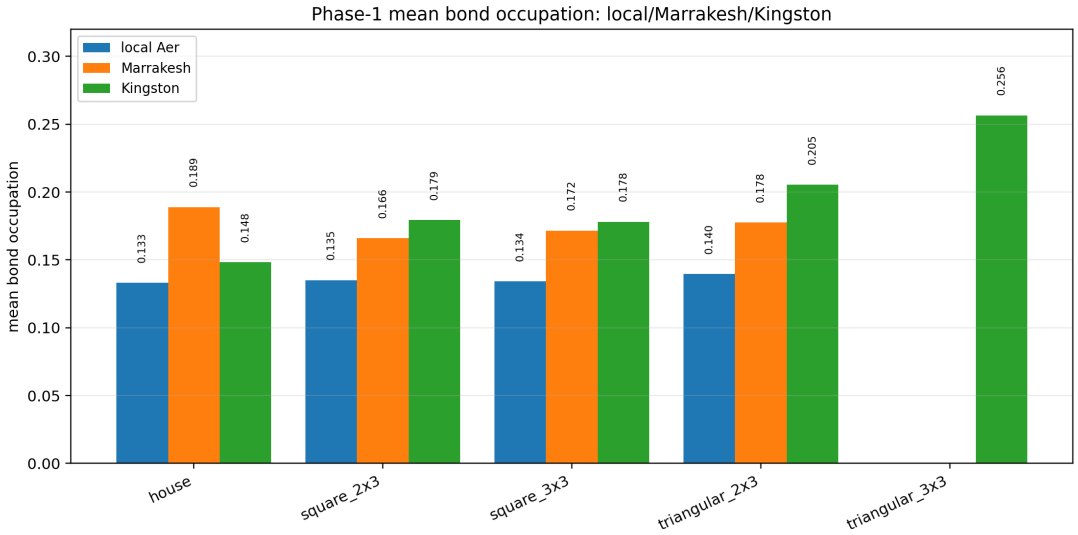

Figure 11: Phase-1A mean bond occupation across local Aer, the first Marrakesh pass, and the Kingston matched-family rerun. The Kingston data add cross-backend robustness, a same-backend house control, and same-backend square and triangular family reach.

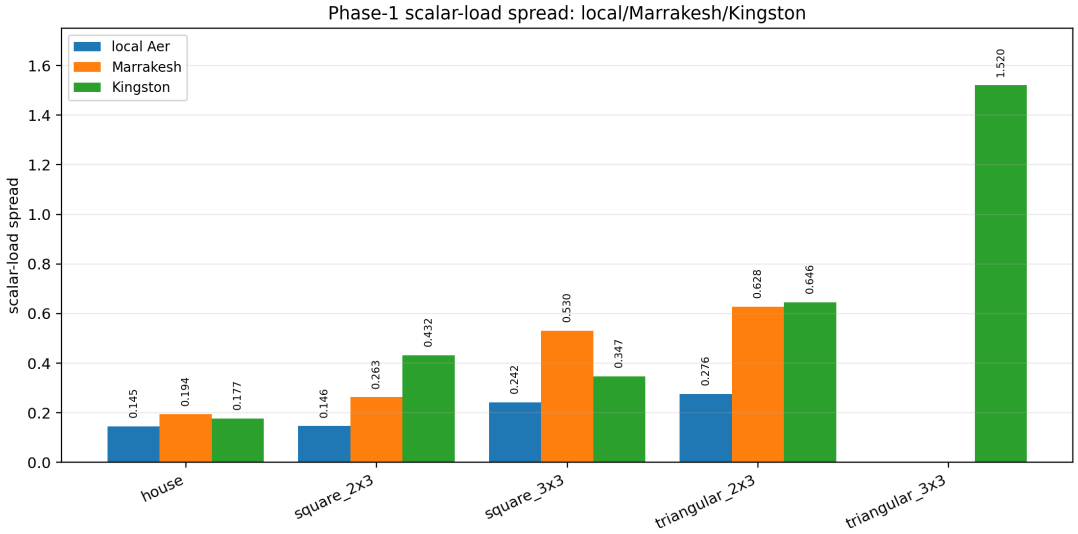

Figure 12: Phase-1A scalar-load spread for the house control, square family, and triangular family across local Aer, Marrakesh, and Kingston. The spread changes across hardware backends and is treated as device- and layout-sensitive, not as a tensor signal. The Kingston `triangular_3x3` point is the largest spread in the current hardware set.

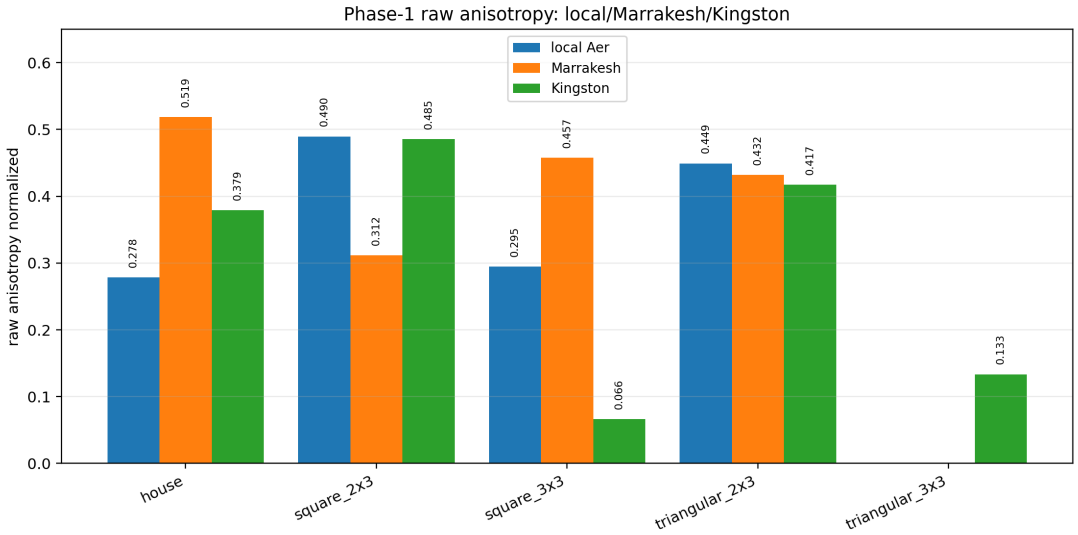

Figure 13: Phase-1A raw anisotropy across local Aer, Marrakesh, and Kingston. The triangular family shows the most interesting same-backend pattern: scalar-load spread grows from `triangular_2x3` to `triangular_3x3`, while normalized raw anisotropy decreases. This flags a follow-up target, not a spin-2 claim.

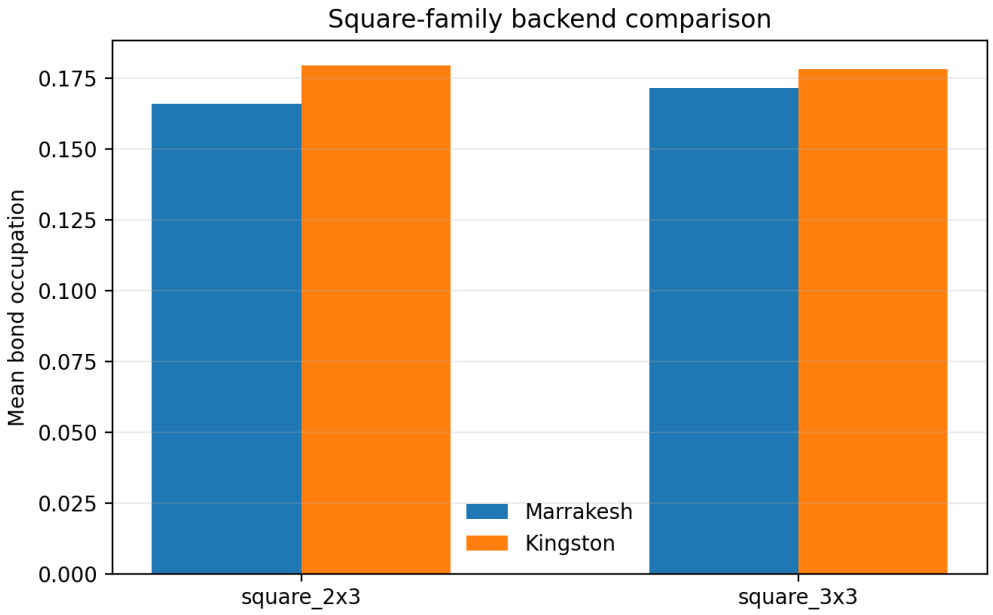

Figure 14: Square-family mean bond occupation for `square_2x3` and `square_3x3`. The near-equal Kingston means are an execution result only; they do not establish scaling or a tensor sector.

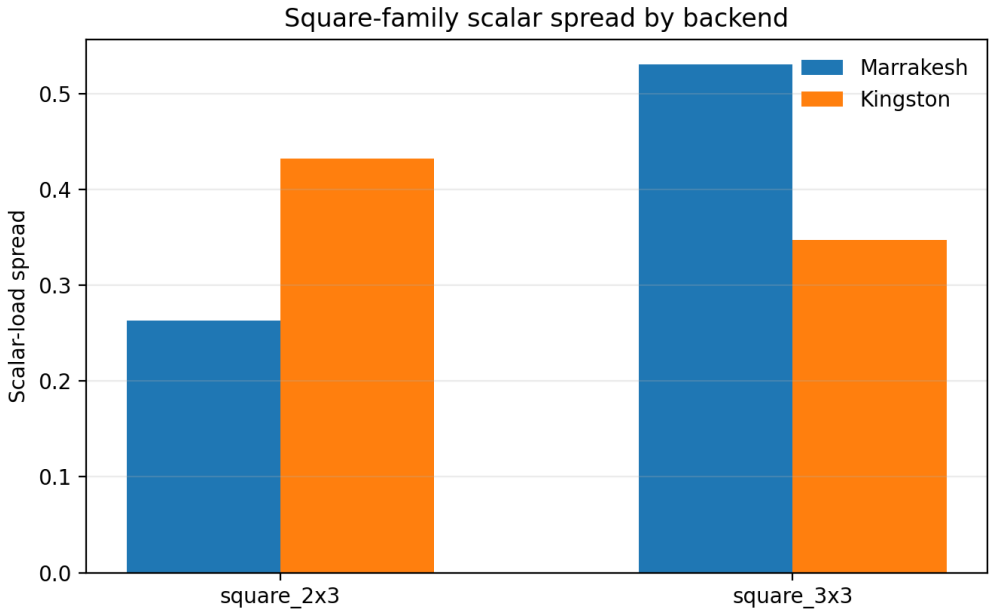

Figure 15: Square-family scalar-load spread. The square-family pair is now available on a single backend, with a house control in the same Kingston pass; repeated layouts and mitigation are still required before any finite-size conclusion can be drawn.

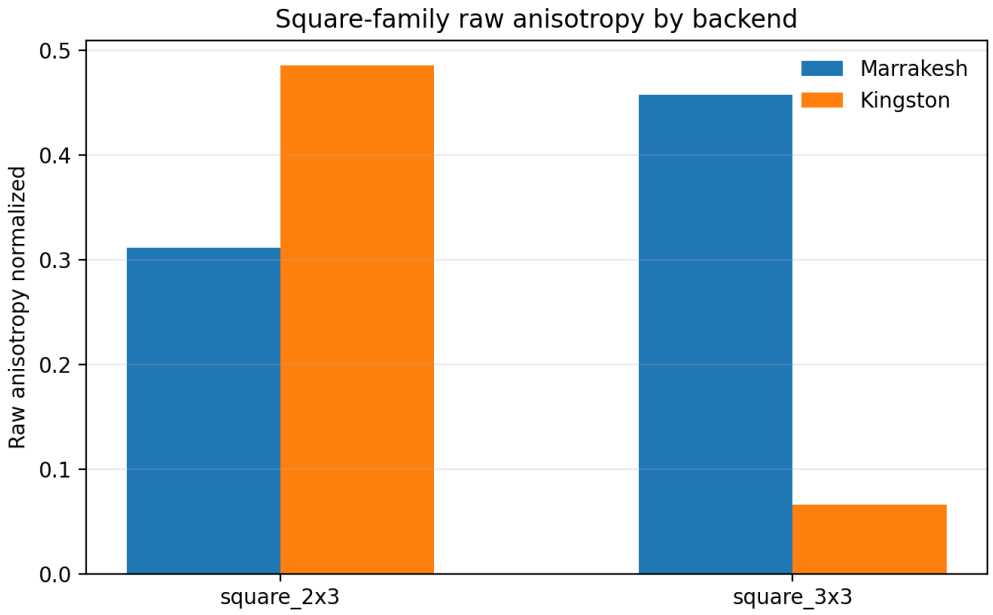

Figure 16: Square-family raw anisotropy. The large change in the Kingston raw anisotropy between `square_2x3` and `square_3x3` is not a spin-2 signal; it flags the need for fixed-layout repeats, tensor-channel observables, and scalar/vector impostor controls.

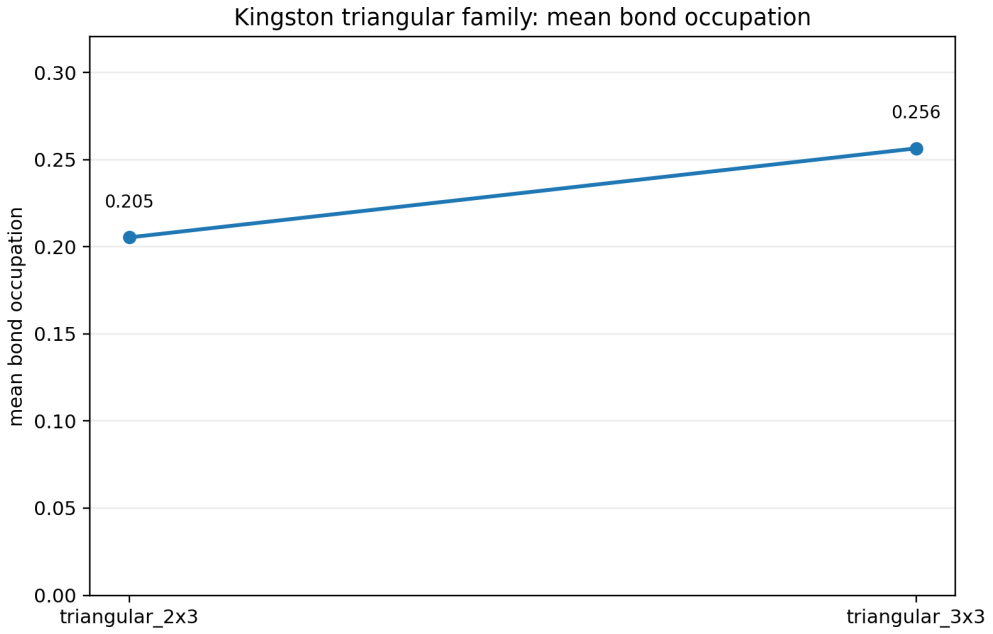

Figure 17: Kingston triangular-family mean bond occupation. The 25-qubit `triangular_3x3` run increases mean bond occupation relative to `triangular_2x3`.

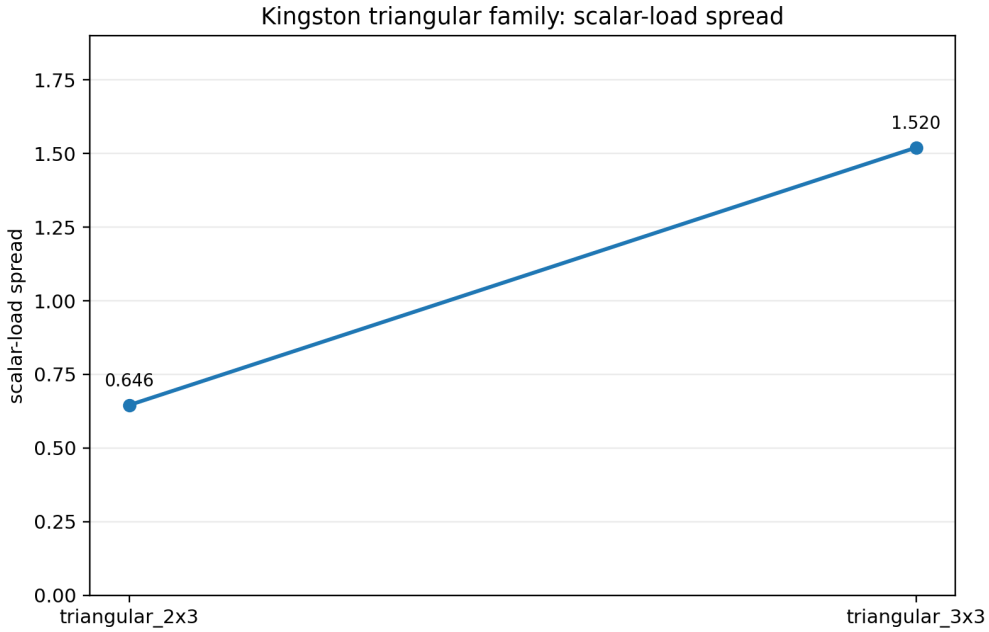

Figure 18: Kingston triangular-family scalar-load spread. The larger triangular graph produces a much larger scalar-load spread in this single hardware batch. The effect is hardware-facing and follow-up-worthy, but not yet interpretable as tensor scaling.

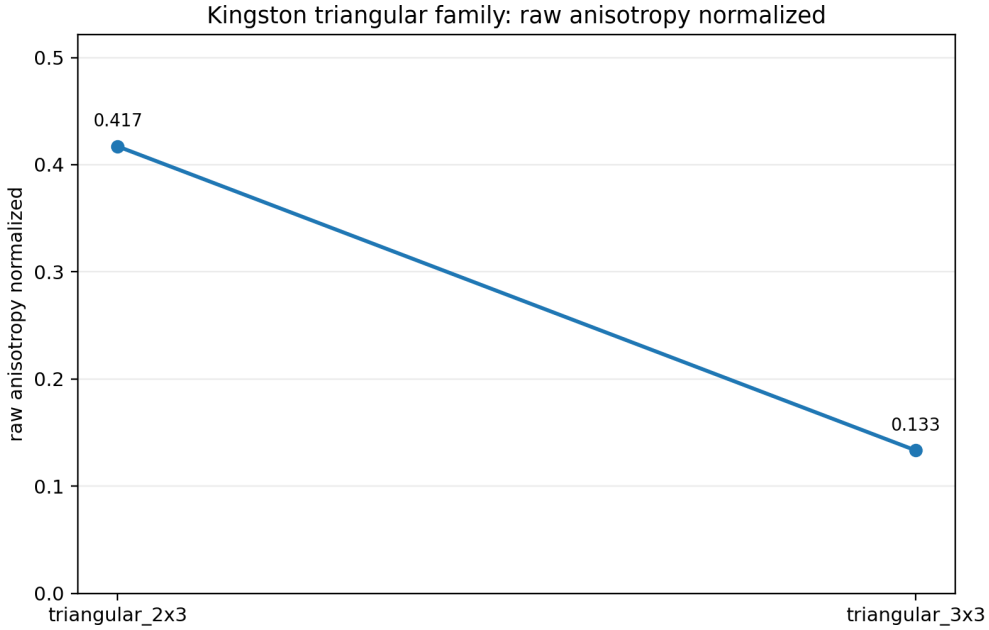

Figure 19: Kingston triangular-family raw anisotropy. Normalized raw anisotropy drops from `triangular_2x3` to `triangular_3x3`, even as scalar-load spread increases. This is the strongest "worth following up" pattern in the current hardware batch, but it remains a raw diagnostic rather than a spin-2 observable.

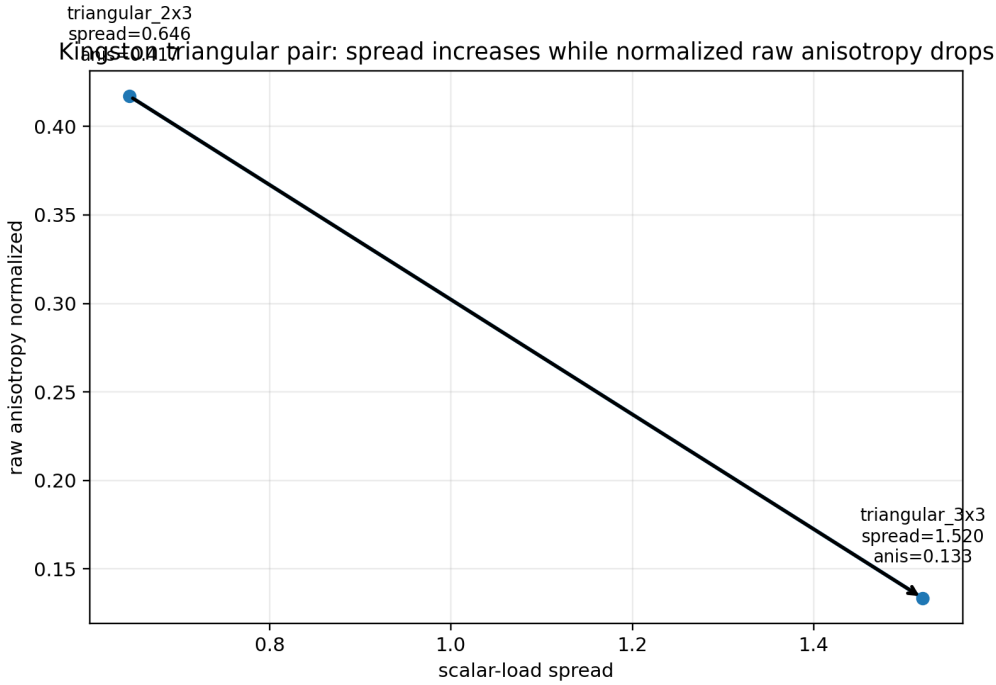

Figure 20: Same-backend triangular-pair summary. The move from `triangular_2x3` to `triangular_3x3` increases scalar-load spread and decreases normalized raw anisotropy. This is the clearest candidate-family follow-up signal, but a Mercury-rung claim still requires fixed-layout repeats, mitigation, tensor susceptibility, Ward-residual checks, and scalar/vector impostor rejection.

15.4 Hardened interpretation of the triangular pair

The Kingston triangular pair is useful, but the dimensional gate changes its status. It is not the correct next spin-2 lane; it is the strongest two-dimensional hardware pipeline-validation result. The hardened standard of this paper is

$$\text{scalar/bond signal} \neq \text{gravity}, \qquad \text{tensor-looking raw anisotropy} \neq \text{spin-2}. \tag{60}$$

Only a pre-registered tensor protocol with scaling, Ward tests, and R_g can pass.

The current triangular result supports four narrower statements. First, `triangular_3x3` is an embedded triangular patch, so the edge directions used for raw anisotropy are part of the circuit family rather than an arbitrary post-hoc chart. Second, it is part of a size pair, `triangular_2x3` $\rightarrow$ `triangular_3x3`. Third, it produced active bond marginals and structured scalar load on real IBM hardware. Fourth, it moved beyond Phase-0A null controls into an admissible embedded-lattice candidate family. These are engineering and protocol advances, not a spin-2 detection.

The run does not yet include the objects required by the tensor protocol:

- no pre-registered fit windows or acceptance thresholds;
- no tensor correlator $S_{ab,cd}(\mathbf{k}, t)$;
- no transverse-traceless fraction F_{TT};
- no effective tensor mass trend $m_g(L)$;

- no Ward/transversality residual $\mathcal{W}(k, L)$;
- no coarse-graining reproduction factor R_{TT};
- no Mercury number $R_g = c_g/c_{\mathrm{clock}}$;
- no fixed physical layout and calibration metadata inside the result record.

The most accurate label is therefore **Phase-1A exploratory hardware candidate result**. It is not "Mercury passed," and it is not "spin-2 observed." It is the first hardware-facing triangular-size pair that is interesting enough to justify a pre-registered tensor repeat.

A Phase-1B repeat should fix the backend, transpiler seed, initial layout, shot count, Trotter settings, readout-mitigation policy, and observables before execution. The first tensor observables should include a primitive orientation-cell tensor map M_{ab}, a structure factor $S_{ab,cd}(\mathbf{k})$, and the diagnostics

$$F_{\mathrm{TT}}(k, L) = \frac{\left\| P^{\mathrm{TT}} S(k, L) P^{\mathrm{TT}} \right\|_F}{\|S(k, L)\|_F}, \tag{61}$$

$$K_{\mathrm{TT}}(0, k; L) \simeq Z^{-1}\left(k^2 + m_g^2(L)\right), \tag{62}$$

$$\mathcal{W}(k, L) = \frac{\|k^a S_{ab,cd}(k, L)\|_F + \|\delta^{ab} S_{ab,cd}(k, L)\|_F}{\|S_{ab,cd}(k, L)\|_F}, \tag{63}$$

$$R_{\mathrm{TT}}(L \to bL) = \mathrm{corr}\Big(P^{\mathrm{TT}} M^{(L)},\, \mathcal{C}_b\left[P^{\mathrm{TT}} M^{(bL)}\right]\Big), \tag{64}$$

where $\mathcal{C}_b$ denotes the chosen coarse-graining map from the larger lattice back to the smaller comparison scale. These quantities are intentionally harder than raw anisotropy. They are the first checks that could distinguish a tensor channel from scalar/vector impostors and hardware layout artifacts.

15.5 Interpretation of Phase 1A

Phase 1A changes the status of the program, but only modestly. The hardware path is no longer restricted to four-qubit negative controls. It now reaches 11–25 qubit non-1D and embedded 2D graph circuits on IBM hardware, including a same-backend Kingston house control plus matched square and triangular graph-family pairs. This is genuine engineering progress. The dimensional gate, however, prevents promoting those embedded sheets into 3+1 spin-2 candidates.

It is not yet physics evidence for an emergent graviton. A Mercury-rung spin-2 statement still requires at least five missing ingredients:

1. a three-dimensional graph family, beginning with a 2x2x2 cubic patch rather than another 2D sheet;
2. a tensor-channel observable beyond scalar loads and raw two-dimensional anisotropy;
3. a measured dynamical exponent z, with $z = 1$ required before any GR-like claim;
4. Ward-residual checks showing suppression of nonphysical polarizations in the infrared;
5. explicit scalar/vector impostor diagnostics, so ordinary bond activation cannot be mistaken for spin-2 emergence.

The correct Phase-1A result statement is therefore:

> *QATNU hardware-readable graph-family circuits now run beyond Phase-0A negative controls. The house motif remains a negative control. The square and triangular em-*

bedded lattices are two-dimensional hardware validation families, not three-dimensional spin-2 admissible substrates. The matched Kingston triangular pair is the strongest two-dimensional hardware-facing signal because ***triangular_3x3*** *increases bond/scalar activation while reducing normalized raw anisotropy relative to* ***triangular_2x3****; nevertheless it is not spin-2 evidence. The next admissible run is a pre-registered 2x2x2 cubic graph.*

16 Reproducibility package

The code package contains exact-simulation utilities, OpenQASM circuits, count analyzers, and real-QPU runners. The Phase-0A exact result is reproduced by

```
cd qatnu_phase0_qpu
python src/run_phase0_exact.py
python src/generate_plots.py
```

The hardware batch is documented in

```
hardware/phase0_qpu/results/hardware_summary.md
```

with backend names, job ids, mean bond occupations, verdicts, claim boundary, and next Mercury-rung requirements. The Phase-1A graph-family pass, including the Kingston house control and matched square and triangular family reruns, is documented in `phase1_graph_families_summary.md` and `phase1_candidate_summary.json`. Individual raw IBM/local count JSON files are intentionally ignored in git; the reproducibility record is the summary plus the analyzer workflow.

A hardware count analysis has the form

```
python src/analyze_counts.py \
  --counts <counts.json> \
  --topology <topology> --N <N>
```

A hardware run command has the form

```
python src/run_ibm_qpu.py \
  --qasm qasm/qatnu_phase0_<topology>_N4.qasm \
  --backend <backend> \
  --shots 2000
```

The expected Phase-0A conclusion is not a positive spin-2 signal. It is an active scalar/bond signal plus structural refusal of the spin-2 claim. The expected Phase-1A conclusion is likewise not a positive spin-2 signal: it is active scalar/bond and raw-anisotropy data on two-dimensional embedded graph families, useful for pipeline validation but not admissible for the 3+1 spin-2 target. The next admissible topology is a three-dimensional cubic patch.

17 What remains to make this a positive spin-2 paper

The Phase-0A and Phase-1A results are gatekeepers and smoke tests, not the destination. A positive spin-2 paper must add the following.

1. **Three-dimensional finite-size graph families.** Stop treating two-dimensional sheets as spin-2 candidates. Begin with a 2x2x2 cubic graph in the same v0 encoding, then extend to 2x2x3 and 3x3x2 under fixed-layout and mitigation policies.
2. **Tensor source response.** Add $J_{ab}M_{ab}$ perturbations and compute $\chi_{ab,cd}$.
3. **Mass/gap and mechanism scan.** Fit $m_2^2(\lambda) = \Delta_B^{(2)} - \lambda^2\Pi_2(0,0)$ where appropriate, but also test for gauge-protected masslessness over a phase rather than only fine-tuned criticality.
4. **Dispersion exponent.** Extract z first. A $z = 2$ or $z = 3$ tensor branch would be a Lifshitz/tensor-medium result, not GR-like spin-2.
5. **Ward residuals.** Show that scalar/vector leakage and trace/divergence residuals decrease in the infrared.
6. **Lorentz recovery.** Only if $z = 1$, extract c_g and report $R_g = c_g/v_{\mathrm{LR}}$ as a Lorentz-recovery diagnostic.

A null result at any step is informative. If a three-dimensional tensor gap never approaches zero, QATNU does not generate a massless tensor in that phase. If the Ward residuals do not vanish, the tensor is a medium mode, not spin-2 gravity. If $z \neq 1$, the result belongs to the Lifshitz lineage rather than to GR. If R_g is not stable after $z = 1$ is established, the model has no emergent Lorentzian limit.

18 Claim registry

The current status is summarized in Table 10. The most important update is that real-QPU execution has moved in two stages: Phase-0A negative controls and Phase-1A embedded graph-family smoke tests. The claim remains narrow.

Table 10: Claim registry for the Mercury rung after Phase-0A and Phase-1 hardware runs.

Claim	Status	Evidence or next test
QATNU is a finite local quantum substrate	Implemented	ED and hardware-readable qubit encodings
Scalar load Λ_i is measurable	Implemented	Exact baselines, IBM Phase-0A batch, and Phase-1A graph families
Scalar timing can be represented by $\omega_{\mathrm{eff}} = \omega/(1+\alpha\Lambda)$	Supported as effective law	Requires larger-system validation
Scalar timing is gravity	Rejected	Scalar sector is holonomy-free and lacks spin-2
Spin-2 target is Pauli-Fierz/TT	Standard benchmark	Known weak-field target
QATNU derives spin-2 unconditionally	Not claimed	Requires tensor criticality and Ward identities

Claim	Status	Evidence or next test
Conditional spin-2 derivation	Revised	Requires 3D infrared limit, measured $z = 1$, chart stability, Ward residuals, and source coupling
Lifshitz spin-2 outcome	Named partial success/failure	Gapless gauge-protected tensor mode with $z \neq 1$; not GR-like gravity
Negative-control exact simulations	Reported result	Corrected Phase-0A structural gate across path, cycle, star, diamond, bowtie
Real-QPU Phase-0A execution	Reported result	IBM path, star, cycle, and diamond controls; all fail expected
Phase-1A graph-family execution	Reported result	IBM house, square_2x3, triangular_2x3, square_3x3, and triangular_3x3 runs; 2D pipeline validation, not 3D spin-2 admissibility
First admissible 3D graph	Not yet run	2x2x2 cubic patch in v0 encoding: 8 vertices, 12 edges, 20 qubits
Path graph spin-2 claim	Rejected structurally	One-dimensional graph, null usable tensor channel, no TT sector
Positive spin-2 sector	Open	Requires admissible graph scaling and $\chi_{ab,cd}$

19 Discussion

The central scientific value of the Mercury rung is that it stops the program from treating every partial resemblance as success. Scalar timing is allowed to be real without being called gravity. Tensor projection is allowed as a diagnostic without being confused for derivation. Negative controls are treated as results rather than embarrassments.

The related-constructions literature makes this discipline more important, not less. It shows that gapless tensor modes can arise in lattice and tensor-gauge settings, but also that the generic controlled outcome need not be relativistic GR. QATNU therefore has to distinguish four levels: scalar/bond activation, raw anisotropy in an embedded chart, a Lifshitz or fracton-like tensor medium, and a true $3 + 1$ Pauli-Fierz sector.

The conditional spin-2 derivation is the bridge between the conceptual program and the next

calculation. It now says exactly what must happen: the admissible graph family must be three-dimensional in the infrared; the tensor susceptibility must exhibit a protected massless branch; the dynamical exponent must be measured rather than assumed; chart dependence must be controlled; and Ward residuals and source coupling must pass independently. If $z \neq 1$, the result may still be valuable, but it belongs to the Lifshitz/tensor-medium family rather than to GR-like gravity. If $z = 1$ but source coupling fails, the result is still not gravity.

The Phase-0A hardware batch is therefore not small in method, even though the graphs are small. It shows that the hardware-readable protocol can produce active scalar/bond observables on real QPUs while the structural gate still refuses false spin-2 interpretations across multiple controls. That is the first requirement for any credible emergence claim: the program must be able to say no before it is trusted when it says maybe.

The Phase-1A graph-family runs add a hardware boundary, not a spin-2 boundary. They show that the hardware path can execute larger embedded two-dimensional families and produce active bond/scalar and raw-anisotropy data. The matched Kingston triangular pair is the most interesting two-dimensional hardware-facing result so far: the larger graph increases mean bond occupation and scalar-load spread while normalized raw anisotropy decreases. But the dimensional gate prevents calling it a spin-2 candidate for the target of this paper. The next scientific boundary is not another two-dimensional repeat; it is the first three-dimensional cubic patch.

20 Conclusion

QATNU now has a Mercury-rung formulation, a real IBM hardware validation layer, and a stricter admissibility standard. The scalar timing sector is defined and bounded. The spin-2 target is stated without projection inflation. The conditional derivation now distinguishes three outcomes that must not be confused: scalar/bond activation, Lifshitz or fracton-like tensor media, and a true 3+1-dimensional Lorentz-recovering Pauli-Fierz sector.

The hardware results remain useful, but their status is narrower than before. Phase 0A shows that small negative controls run on real IBM QPUs while remaining structurally rejected. Phase 1A shows that larger house, square, and triangular circuits also run and produce active bond/scalar and raw-anisotropy observables. The matched Kingston triangular pair is the strongest hardware-facing two-dimensional signal so far: mean bond occupation and scalar-load spread increase from `triangular_2x3` to `triangular_3x3`, while normalized raw anisotropy drops. But the spatial-dimension gate forbids promoting that result into a spin-2 candidate for 3+1-dimensional gravity. A two-dimensional sheet has zero local graviton polarizations for the target theory.

The next paper should not repeat two-dimensional hardware smoke tests unless they are used as noise or pipeline controls. It should move to Phase 1B: a pre-registered 2x2x2 cubic QATNU run with fixed backend, fixed transpiler seed, captured layout, calibration metadata, mitigation policy, and fixed observables. The first measured quantity should be the dispersion exponent z or, at smaller scale, the finite-size proxy for whether the tensor gap closes consistently with a 3D continuum. If $z \neq 1$, QATNU has joined the Lifshitz/tensor-medium lineage. If $z = 1$, the next gates are chart stability, Ward residuals, source coupling, and only then $R_g = c_g/v_{\mathrm{LR}}$.

A Hardware run prompt

Run or reproduce the QATNU Mercury-rung hardware sequence with the corrected dimensional gate. Phase-0A path, star, cycle, and diamond circuits are negative controls. Phase-1A house, square, and triangular circuits are two-dimensional pipeline-validation tests, not 3D spin-2 candidates. Save raw bitstring counts with backend name, job id, shot count, layout/transpilation metadata, and calibration date if available, and analyze mean bond occupation, scalar-load spread, and raw anisotropy.

For the next admissible Mercury-rung run, generate a 2x2x2 cubic QATNU circuit in the v0 encoding: 8 matter qubits plus 12 bond qubits, 20 hardware qubits total. Use fixed backend, fixed transpiler seed, captured physical layout, a declared mitigation policy, and pre-registered observables. Report scalar/bond observables as pipeline checks, but do not claim spin-2 unless the 3D tensor protocol measures a tensor susceptibility, finite-size tensor mass/gap trend, dynamical exponent z, chart stability, Ward residuals, and scalar/vector impostor rejection. If $z = 1$, compute c_g and $R_g = c_g/v_{\mathrm{LR}}$ as Lorentz-recovery diagnostics.

B Notation

Symbol	Meaning	Status
H_{micro}	Microscopic QATNU Hamiltonian	Finite graph substrate
Λ_i	Internal scalar load at vertex i	Measured in exact, IBM Phase-0A, and Phase-1A graph-family runs where counts are available
L_w	Weighted graph Laplacian	Scalar closure operator
M_{ab}	Bond-stress tensor candidate	Spin-2 observable candidate
$K_{ab,cd}$	Inverse tensor susceptibility	Future tensor test
m_2^2	Tensor mass parameter	Criticality target
Z_2, ρ_2	Tensor kinetic and stiffness coefficients	Determine c_g
c_g	Emergent tensor-wave speed	Future output
v_{LR}	Lieb-Robinson / substrate causal-cone velocity	Defines Lorentz-recovery diagnostic
R_g	c_g/v_{LR}	Lorentz-recovery diagnostic after $z = 1$ is established
$\mathcal{W}_{\mathrm{div}}, \mathcal{W}_{\mathrm{tr}}$	Ward residuals	Gauge/constraint diagnostics

C References

1. A. Einstein, “Die Feldgleichungen der Gravitation,” Sitzungsberichte der Preussischen Akademie der Wissenschaften, 1915.
2. M. Fierz and W. Pauli, “On relativistic wave equations for particles of arbitrary spin in an electromagnetic field,” Proceedings of the Royal Society A, 1939.

3. S. Weinberg, "Photons and gravitons in perturbation theory: Derivation of Maxwell's and Einstein's equations," Physical Review, 1965.
4. S. Weinberg and E. Witten, "Limits on massless particles," Physics Letters B, 1980.
5. E. H. Lieb and D. W. Robinson, "The finite group velocity of quantum spin systems," Communications in Mathematical Physics, 1972.
6. Z.-C. Gu and X.-G. Wen, "Emergence of helicity ±2 modes (gravitons) from qubit models," Nuclear Physics B 863, 90–129, 2012; arXiv:0907.1203.
7. Z.-C. Gu and X.-G. Wen, "A lattice bosonic model as a quantum theory of gravity," arXiv:gr-qc/0606100.
8. C. Xu, "Novel algebraic boson liquid phase with soft graviton excitations," Physical Review B 74, 224433, 2006.
9. C. Xu and P. Hořava, "Emergent gravity at a Lifshitz point from a Bose liquid on the lattice," Physical Review D 81, 104033, 2010.
10. M. Pretko, "Emergent gravity of fractons: Mach's principle revisited," Physical Review D 96, 024051, 2017.
11. M. Pretko and L. Radzihovsky, "Fracton-elasticity duality," Physical Review Letters 120, 195301, 2018.
12. S. Deser, R. Jackiw, and G. 't Hooft, "Three-dimensional Einstein gravity: dynamics of flat space," Annals of Physics 152, 220–235, 1984.
13. E. Witten, "(2+1)-dimensional gravity as an exactly soluble system," Nuclear Physics B 311, 46–78, 1988.
14. H. van Dam and M. Veltman, "Massive and massless Yang-Mills and gravitational fields," Nuclear Physics B 22, 397–411, 1970.
15. V. I. Zakharov, "Linearized gravitation theory and the graviton mass," JETP Letters 12, 312, 1970.
16. C. W. Misner, K. S. Thorne, and J. A. Wheeler, *Gravitation.* W. H. Freeman, 1973.
17. R. M. Wald, *General Relativity.* University of Chicago Press, 1984.
18. IBM Quantum Documentation, Qiskit Runtime and IBM Quantum Platform documentation, accessed May 2026. https://quantum.cloud.ibm.com/docs
19. PyQuafu Documentation, "Welcome to PyQuafu's documentation," accessed May 2026. https://scq-cloud.github.io/
20. PyQuafu Documentation, "User guide," accessed May 2026. https://scq-cloud.github.io/0.2.x/index.html